



Selective formation of large-grained, (100)- or (111)-oriented Si on glass by Al-induced layer exchange

K. Toko, R. Numata, N. Saitoh, N. Yoshizawa, N. Usami, and T. Suemasu

Citation: [Journal of Applied Physics](#) **115**, 094301 (2014); doi: 10.1063/1.4867218

View online: <http://dx.doi.org/10.1063/1.4867218>

View Table of Contents: <http://scitation.aip.org/content/aip/journal/jap/115/9?ver=pdfcov>

Published by the [AIP Publishing](#)



Re-register for Table of Content Alerts

Create a profile.



Sign up today!



Selective formation of large-grained, (100)- or (111)-oriented Si on glass by Al-induced layer exchange

K. Toko,^{1,a)} R. Numata,¹ N. Saitoh,² N. Yoshizawa,² N. Usami,³ and T. Suemasu¹

¹*Institute of Applied Physics, University of Tsukuba, 1-1-1 Tennodai, Tsukuba, Ibaraki 305-8573, Japan*

²*Electron Microscope Facility, TIA, AIST, 16-1 Onogawa, Tsukuba 305-8569, Japan*

³*Materials, Physics and Energy Engineering, Nagoya University, Aichi 464-8603, Japan*

(Received 19 January 2014; accepted 18 February 2014; published online 3 March 2014)

By controlling the Si thickness and the annealing temperature used for Al-induced crystallization, we controlled the fraction of (100) and (111) orientations of polycrystalline Si (poly-Si) grains grown on glass. Changing the proportions of crystal orientation strongly influenced the average grain size of the poly-Si layer. By growing a 99% (111)-oriented poly-Si layer, formed with a 50-nm-thick Si layer at 375 °C, we produced a Si layer with grains nearly 40 μm in size. We discuss the growth mechanism from the perspective of competition between (100)- and (111)-oriented nuclei. This achievement holds promise for fabricating high-efficiency thin-film solar cells on inexpensive glass substrates. © 2014 AIP Publishing LLC. [<http://dx.doi.org/10.1063/1.4867218>]

I. INTRODUCTION

Forming large-grained polycrystalline Si (poly-Si) on glass at low temperatures has been widely studied for fabricating inexpensive thin-film solar cells with high-conversion efficiencies, because poly-Si cells with sufficiently large grains (>10 μm) can exhibit efficiencies nearly that of cells made from single-crystalline Si.^{1–3} Besides, orientation-controlled poly-Si layers are essential for fabricating antireflective structures, controlled nanostructures, and tandem structures with advanced materials.^{4–6}

Al-induced crystallization (AIC) has gained much attention as a way to form poly-Si on glass below the softening temperature of glass (~550 °C). In this technique, an amorphous Si (a-Si) layer on Al is crystallized by exchanges between the Al and Si layers during annealing (425–500 °C).^{7–13} AIC allows for orientation control in large-grained poly-Si layers.^{14–17} Because the AIC-Si layer is doped p-type from residual Al atoms in the Si layer, researchers expect it to be useful as a seed layer for growth of a Si light-absorption layer by epitaxial thickening techniques.^{2,18–20}

Fabricating the solar cell and characterizing its electrical properties both require a conducting layer under the poly-Si layer. To accomplish this, some researchers have investigated AIC of a-Si on conducting layers,²¹ while others have investigated inverted AIC.^{7,22–24} Inverted AIC begins with an Al/a-Si/substrate structure, contrasting the a-Si/Al/substrate structure used in normal AIC. During annealing, an Al conducting layer forms under the poly-Si layer via self-organizing layer exchange. In an earlier report, we found that the crystal orientation of the poly-Si layer strongly depended on the thicknesses of the original Si and Al layers.²⁵ However, it remains uncertain what parameters influence the grain size of the poly-Si layer, one of the most important factors for thin-film solar cells. In this paper, we performed inverted AIC of a-Si and studied the correlation

between the crystal orientation and the grain size; from these results, we discuss a way to enlarge the grain size in the poly-Si layer, promising for designing high-efficiency poly-Si thin-film solar cells.

II. EXPERIMENT

Amorphous Si layers [thickness (t_{Si}): 50–400 nm] were prepared on SiO₂ glass substrates. SiO₂ membranes were prepared on the a-Si layers by sequentially dipping the samples in ammonium hydrogen-peroxide mixture solution (NH₄OH:H₂O₂:H₂O = 1:1:10) for 30 min at 80 °C. Al layers with the same thickness as the a-Si layers were then prepared on the SiO₂ membranes. Si and Al were deposited at room temperature by using RF magnetron sputtering with Ar plasma. The samples were then annealed at temperatures (T_a) of 325–450 °C in N₂ ambient for 1–100 h. Figure 1(a) shows a schematic of the sample structure. During annealing, the surface morphology of each sample was observed by using Nomarski optical microscopy. The crystal orientations and the grain sizes of the resulting poly-Si layers were characterized by electron backscatter diffraction (EBSD) analysis. Prior to the EBSD measurements, the surface of the poly-Si layer was cleaned using a diluted HF solution (1.5% HF) for 1 min. The detailed crystal structure was observed using a FEI Tecnai Osiris transmission electron microscope (TEM), operated at 200 kV, and a TOPCON EM-002B TEM, operated at 120 kV. Elemental composition profiles were measured with a high-angle annular dark-field (HAADF) scanning transmission electron microscope (STEM) with a probe diameter of ~1 nm, as well as with an energy-dispersive x-ray spectrometer (EDX). Cross-sectional TEM samples were prepared by milling with a focused ion beam.

III. RESULTS AND DISCUSSIONS

Figures 1(b)–1(d) show Nomarski optical micrographs of the sample with $t_{Si} = 50$ nm, $T_a = 325$ °C, revealing how its morphology changed over time. During annealing, the Si

^{a)}E-mail address: toko@bk.tsukuba.ac.jp

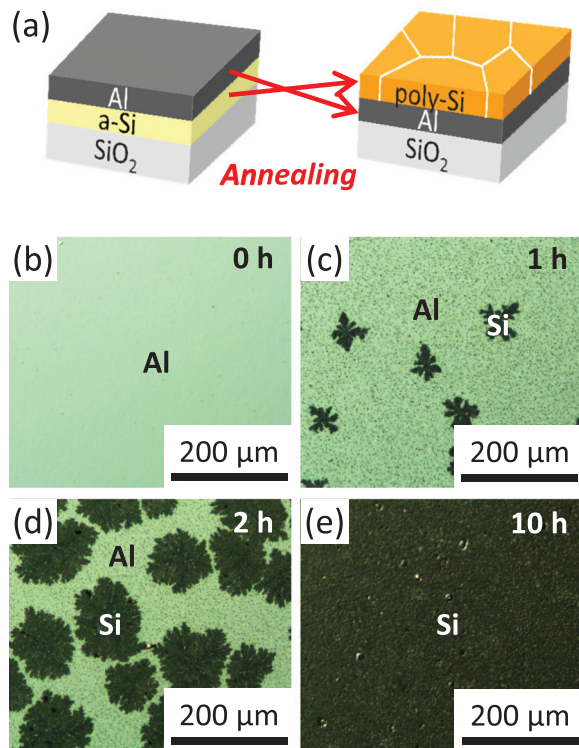


FIG. 1. (a) Schematic of layer exchange during inverted AIC of a-Si. (b)–(e) Nomarski optical micrographs of the 100-nm-thick sample, annealed at 425 °C for (b) 0 h, (c) 1 h, (d) 2 h, and (e) 10 h; the dark area corresponds to Si, while the bright area corresponds to Al.

atoms diffused to the Al layer, grew laterally, and then covered the entire surface of the sample. This surface morphology is almost identical to the morphology of the back surface in AIC samples, observed through transparent SiO₂ substrates.^{14–17}

Figure 2 shows crystal-orientation maps of the poly-Si layers in a matrix of T_a and t_{Si} . For the sample with $t_{Si} = 50$ nm, $T_a = 325$ °C, layer exchange did not finish within 100 h. We attribute this low growth rate to the difficulty of layer exchange, as described in our previous study on AIC-Ge.²⁶ The crystal orientation clearly depended on t_{Si} : (111) was dominant for small t_{Si} [Figs. 2(a) and 2(b)], while (100) was dominant for large t_{Si} [Figs. 2(f)–2(h)]. Note that, in the 100-nm-thick sample, the crystal orientation clearly depended on T_a : (111) was dominant for small T_a [Fig. 2(c)], while (100) was dominant for large T_a [Fig. 2(e)].

Using EBSD analysis, we calculated the fractions of crystal orientations in the poly-Si layers as a function of T_a , summarized in Figs. 3(a) and 3(b). By definition, the (100) and (111) fractions contain planes with tilts up to 15° from the exact (100) and (111) planes, respectively. For all samples (t_{Si} : 50, 100, 200, 300, and 400 nm), the (100) fraction increased with increasing T_a , while the (111) fraction increased with decreasing T_a . The greatest orientation fractions were 88% (100) for the sample with $t_{Si} = 200$ nm, $T_a = 425$ °C and 99% (111) for the sample with $t_{Si} = 50$ nm, $T_a = 375$ °C. Thus, using different t_{Si} and T_a in inverted AIC controls the crystal orientation of the poly-Si layer, between the (100) and (111) planes. Changing T_a most strongly affected crystal orientation in the sample with $t_{Si} = 100$ nm, which has lower orientation compared to the other samples.

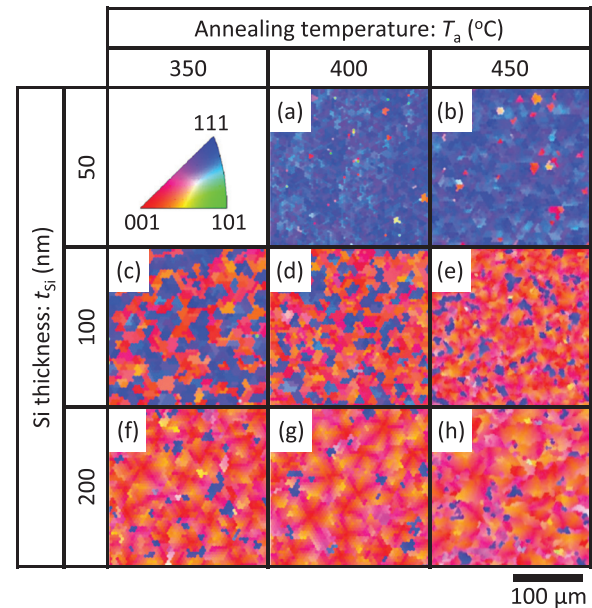


FIG. 2. (a)–(h) EBSD images of inverted-AIC-Si layers, summarized as a matrix of T_a (350, 400, and 450 °C) and t_{Si} (50, 100, and 200 nm). Coloration indicates crystal orientation, according to the legend.

We used EBSD analysis to determine the average grain size of the poly-Si layers, summarized in Fig. 3(c) as a function of T_a . The grain size decreased with increasing T_a for the sample with $t_{Si} = 50$ nm, while the samples with $t_{Si} = 200$ –400 nm exhibited the opposite behavior. In contrast, the grain size of the sample with $t_{Si} = 100$ nm did not depend on T_a . Thus, how grain size depended on T_a differed

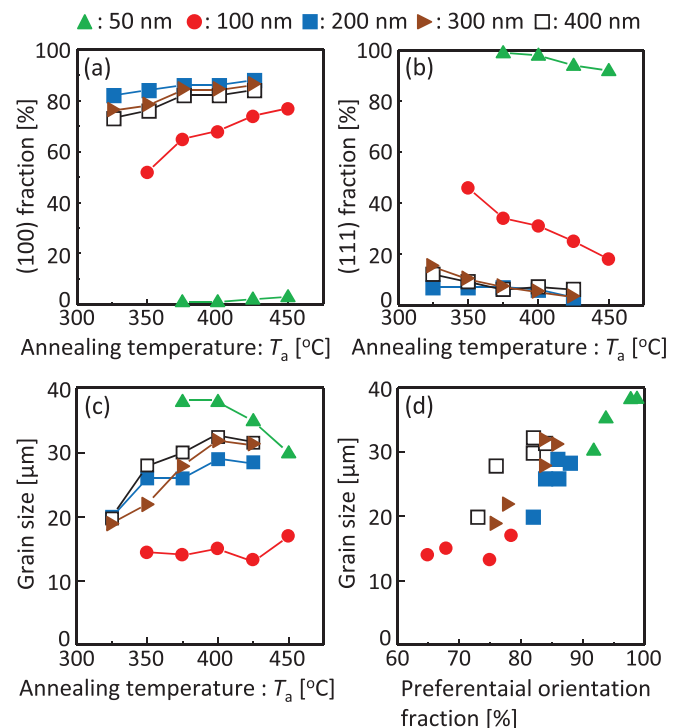


FIG. 3. EBSD characterization of the inverted-AIC-Si layers with $t_{Si} = 50$, 100, 200, 300, and 400 nm, showing how various properties depended on annealing temperature: (a) fraction of (100) orientation, (b) fraction of (111) orientation, and (c) average grain size. (d) Average grain size as a function of the fraction of preferential orientation [i.e., (100) or (111)].

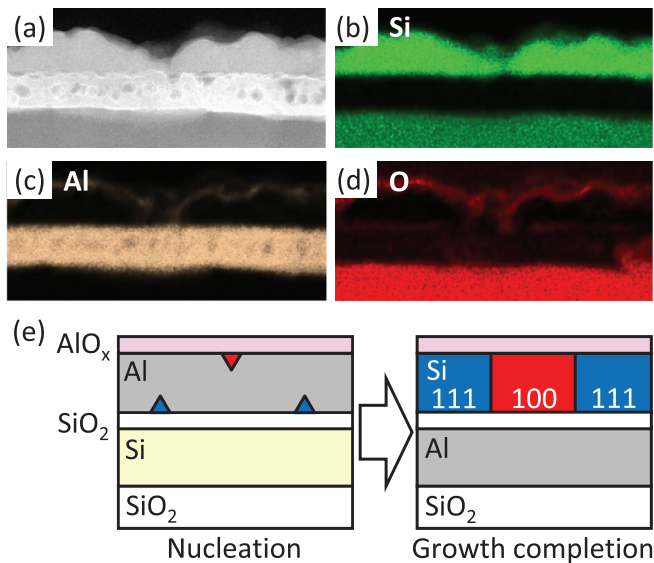


FIG. 4. Cross-sectional TEM micrographs and analysis of the sample with $t_{\text{Si}} = 50 \text{ nm}$, $T_a = 375 \text{ }^\circ\text{C}$. (a) STEM-HAADF micrograph. (b)–(d) EDX elemental maps of (b) Si, (c) Al, and (d) O from the region shown in (a). (e) Schematic of nucleation-site-dependent crystal orientation during inverted AIC.

based on t_{Si} , whereas how crystal orientation depended on T_a was the same for all samples. Figure 3(d) shows the average grain size of the poly-Si layers as a function of the fraction of preferential orientation, showing that the higher fraction of the preferential orientation leads to a larger average grain size. This result shows that controlling the orientation is an effective way to increase the grain size in poly-Si layers formed by AIC.

The dominance of (100)- or (111)-oriented grains in the AIC-Si layers can be explained from the perspective of nucleation sites. Figures 4(a)–4(d) prove the stacked Si/Al/SiO₂ structure of the inverted-AIC sample (t_{Si} : 50 nm, T_a : 375 °C). Figures 4(c) and 4(d) show the presence of a native AlO_x layer on the Si surface, which was formed before layer exchange began. Figure 4(d) suggests that the SiO₂ diffusion-limiting layer, purposely formed during sample preparation, remained between the Si and Al layers. The nuclei of group-IV semiconductors are preferentially oriented to (100) on AlO_x and to (111) on SiO₂, caused by minimization of interfacial energy.^{16,27,28} These orientations may explain why the AIC-Si layers consisted of only (100)- or (111)-oriented grains, as shown in Fig. 2. The dependence of crystal orientation on t_{Si} and T_a in the inverted-AIC-Si layer depends on the extent of supersaturation of Si in Al, which is the driving force of the Si nucleation. In the AIC process, the supersaturation level of Si in Al increases for smaller volumes (i.e., thicknesses) of Si/Al and lower annealing temperatures.¹⁶ At high levels of supersaturation, the Al layer likely splits the Si nuclei on a dense plane, i.e., the (111)-oriented Si nuclei, to reduce the Si concentration in Al. Because changing t_{Si} and T_a change the supersaturation level of Si in Al, they also determine the orientation of the nucleating Si: (111) on SiO₂ or (100) on AlO_x.

Based on this growth model, we can explain how controlling the orientation can change the grain size of the poly-Si layer grown by AIC, enabling larger grain sizes. Figure

4(e) shows a situation where Si can nucleate on both the AlO_x and SiO₂ layers. This situation leads to higher nucleation density as well as smaller grain size, because of competition between the (100)- and (111)-oriented nuclei. Thus, limiting the nucleation site, i.e., controlling the orientation to either (100) or (111), is essential for increasing the grain size of the AIC-Si layers.

Figure 5(a) shows a representative bright-field TEM image of the sample with $t_{\text{Si}} = 50 \text{ nm}$, $T_a = 375 \text{ }^\circ\text{C}$, which has the largest grain size ($\sim 40 \mu\text{m}$) among the samples. Figures 5(b) and 5(c) show dark-field TEM images, using the Si {111} plane reflection, taken to characterize defects in the poly-Si layer. In the Si layer processed for TEM ($\sim 7.3 \mu\text{m}$ width), most regions contained no obvious defects [Fig. 5(b)], while a few regions contained some defects, including stacking faults [Fig. 5(c)]; note that TEM did not reveal disordered grain boundaries. Figures 5(d) and 5(e) show the selected-area electron-diffraction (SAED) patterns and the g-vector, respectively, taken from the region shown in Fig. 5(c). In both regions, the Si {111} direction was almost perpendicular to the substrate, demonstrating that the poly-Si layer consisted of large, (111)-oriented grains, a result which

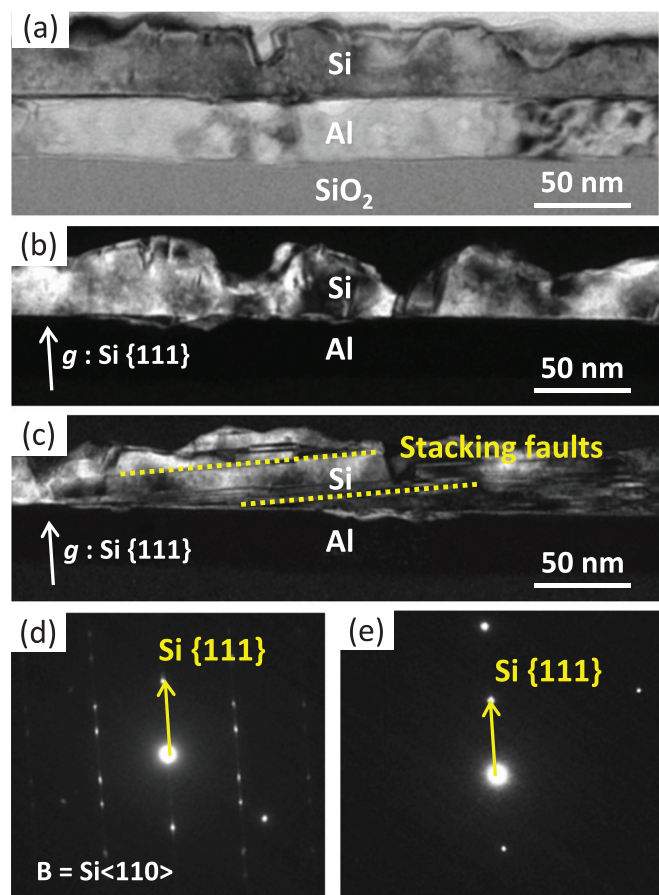


FIG. 5. Detailed TEM crystal structure of the sample with $t_{\text{Si}} = 50 \text{ nm}$, $T_a = 375 \text{ }^\circ\text{C}$. (a) Representative bright-field image. (b)–(c) Dark-field images using the Si {111} plane reflection showing single-crystal structures (b) without any defects and (c) with some defects, including a stacking fault. Typical stacking faults are indicated by yellow dotted lines. (d)–(e) SAED patterns showing the (d) Si{110} zone axis and the (e) g-vector, taken from the dark-field image shown in (c).

agrees with the EBSD measurement. Figure 5(d) also shows a twinned Si structure and some streaking along the Si (111) direction, caused by planar defects in the Si{111} planes. Because these defects were parallel to the substrate, no defects appeared on the Si surface. Thus, this Si layer is a promising epitaxial template for light-absorbing, low-defect Si layers and other advanced functional materials.

IV. CONCLUSION

By using AIC, we selectively formed large-grained, (100)- and (111)-oriented Si on glass by controlling the annealing temperature and the Si thickness. We found that higher fractions of the preferential orientation led to a larger average grain size in the resulting poly-Si layer. Using this trend, we formed a 99% (111)-oriented Si layer with a large grain size ($\sim 40 \mu\text{m}$) at a low temperature of 375°C . These findings hold promise for developing high-efficiency thin-film solar cells on inexpensive glass substrates.

ACKNOWLEDGMENTS

This work was partially supported by a Grant-in-Aid for Scientific Research from the Ministry of Education, Culture, Sport, Science, and Technology in Japan and the Yazaki Memorial Foundation for Science and Technology.

¹M. A. Green, *Sol. Energy* **74**, 181 (2003).

²W. Fuhs, S. Gall, B. Rau, M. Schmidt, and J. Schneider, *Sol. Energy* **77**, 961 (2004).

³M. Imaizumi, T. Ito, M. Yamaguchi, and K. Kaneko, *J. Appl. Phys.* **81**, 7635 (1997).

⁴P. Campbell, S. R. Wenham, and M. A. Green, *Sol. Energy Mater. Sol. Cells* **31**, 133 (1993).

⁵Y. Cohin, O. Mauguin, L. Largeau, G. Patriarche, F. Glas, E. Søndergård, and J.-C. Harmand, *Nano Lett.* **13**, 2743 (2013).

⁶D. Tsukada, Y. Matsumoto, R. Sasaki, M. Takeishi, T. Saito, N. Usami, and T. Suemasu, *Appl. Phys. Express* **2**, 051601 (2009).

⁷O. Nast and A. J. Hartmann, *J. Appl. Phys.* **88**, 716 (2000).

⁸Y. Sugimoto, N. Takata, T. Hirota, K. Ikeda, F. Yoshida, H. Nakashima, and H. Nakashima, *Jpn. J. Appl. Phys., Part 1* **44**, 4770 (2005).

⁹J. Y. Wang, Z. M. Wang, and E. J. Mittemeijer, *J. Appl. Phys.* **102**, 113523 (2007).

¹⁰B. I. Birajdar, T. Antesberger, B. Butz, M. Stutzmann, and E. Spiecker, *Scr. Mater.* **66**, 550 (2012).

¹¹O. Ebil, R. Aparicio, and R. Birkmire, *Thin Solid Films* **519**, 178 (2010).

¹²C. C. Peng, C. K. Chung, and J. F. Lin, *Acta Mater.* **59**, 6093 (2011).

¹³S. Y. Wei, S. M. Yu, L. C. Yu, W. C. Sun, C. K. Hsieh, T. S. Lin, C. H. Tsai, and F. R. Chen, *Cryst. Eng. Commun.* **14**, 4967 (2012).

¹⁴M. Kurosawa, N. Kawabata, T. Sadoh, and M. Miyao, *Appl. Phys. Lett.* **95**, 132103 (2009).

¹⁵M. Jung, A. Okada, T. Saito, T. Suemasu, and N. Usami, *Appl. Phys. Express* **3**, 095803 (2010).

¹⁶A. Sarikov, J. Schneider, J. Berghold, M. Muske, I. Sieber, S. Gall, and W. Fuhs, *J. Appl. Phys.* **107**, 114318 (2010).

¹⁷A. Okada, K. Toko, K. O. Hara, N. Usami, and T. Suemasu, *J. Cryst. Growth* **356**, 65 (2012).

¹⁸P. I. Widenborg, A. Straub, and A. G. Aberle, *J. Cryst. Growth* **276**, 19 (2005).

¹⁹I. Gordon, L. Carnel, D. Van Gestel, G. Beaucarne, and J. Poortmans, *Thin Solid Films* **516**, 6984 (2008).

²⁰B. R. Wu, S. Y. Lo, D. S. Wu, S. L. Ou, H. Y. Mao, J. H. Wang, and R. H. Horng, *Thin Solid Films* **520**, 5860 (2012).

²¹K. Y. Lee, C. Becker, M. Muske, F. Ruske, S. Gall, B. Rech, M. Berginski, and J. Huüpkens, *Appl. Phys. Lett.* **91**, 241911 (2007).

²²G. Ekanayake, T. Quinn, and H. S. Reehal, *J. Cryst. Growth* **293**, 351 (2006).

²³H. Kuraseko, N. Orita, H. Koaizawa, and M. Kondo, *Appl. Phys. Express* **2**, 015501 (2009).

²⁴C. Jaeger, M. Bator, S. Matich, and M. Stutzmann, *J. Appl. Phys.* **108**, 113513 (2010).

²⁵R. Numata, K. Toko, N. Saitoh, N. Yoshizawa, N. Usami, and T. Suemasu, *Cryst. Growth Des.* **13**, 1767 (2013).

²⁶K. Nakazawa, K. Toko, N. Usami, and T. Suemasu, *ESC J. Solid State Sci. Technol.* **2**, Q195 (2013).

²⁷J.-H. Park, T. Suzuki, M. Kurosawa, M. Miyao, and T. Sadoh, *Appl. Phys. Lett.* **103**, 082102 (2013).

²⁸A. A. Stekolnikov, J. Furthmüller, and F. Bechstedt, *Phys. Rev. B* **65**, 115318 (2002).